International Journal of Automotive Technology, Vol. 5, No. 3, pp. 155–164 (2004)

1229–9138/2004/017–02

CHARACTERISTICS OF WALL IMPINGEMENT AT ELEVATED TEMPERATURE CONDITIONS ON GDI SPRAY

J. PARK, K.-S. IM*, H. KIM and M.-C. LAI

Mechanical Engineering Department, Wayne State University,
5050 Anthony Wayne Drive Detroit, Michigan 48202, U.S.A.

(Received 19 September 2003; Revised 16 February 2004)

ABSTRACT–The direct injection gasoline spray-wall interaction was characterized inside a heated pressurized chamber using various visualization techniques, including high-speed laser-sheet macroscopic and microscopic movies up to 25,000 frames per second, shadowgraph, and double-spark particle image velocimetry. Two hollow cone high-pressure swirl injectors having different cone angles were used to inject gasoline onto a heated plate at two different impingement angles. Based on the visualization results, the overall transient spray impingement structure, fuel film formation, and preliminary droplet size and velocity were analyzed. The results show that upward spray vortex inside the spray is more obvious at elevated temperature condition, particularly for the wide-cone-angle injector, due to the vaporization of small droplets and decreased air density. Film build-up on the surface is clearly observed at both ambient and elevated temperature, especially for narrow cone spray. Vapor phase appears at both ambient and elevated temperature conditions, particularly in the toroidal vortex and impingement plume. More rapid impingement and faster horizontal spread after impingement are observed for elevated temperature conditions. Droplet rebounding and film break-up are clearly observed. Post-impingement droplets are significantly smaller than pre-impingement droplets with a more horizontal velocity component regardless of the wall temperature and impingement angle condition.

KEY WORDS : Impingement, Direct injection, Visualization, Shadowgraph

1. INTRODUCTION

The interaction between the fuel sprays and solid combustion chamber walls is a very important issue in all internal combustion engines utilizing direct fuel injection, especially for small-bore engines used in passenger cars. Previous researchers have focused on the spray impingement in diesel engines (e.g., Nabers *et al.*, 1988; 1993) and port-fuel-injection (PFI) engines (e.g., Senda *et al.*, 1999; Kim *et al.*, 2004), but there are very few experimental papers on high-pressure gasoline spray wall interactions for gasoline direct injection spark ignition (DISI) engines (Yoo *et al.*, 1998). Spray impingement in DISI engines must be studied in its own class since its fuel, spray structure and injection pressure are different from those of diesel and PFI engines.

DISI engine is of great interest to the automotive industry because of its potentially better fuel economy compared to PFI engines (Zhao *et al.*, 1997). DISI engine, however, has a number of inherent emission problems such as high light-load UBHC and even particulate emissions with late fuel injection. The emissions are strongly affected by the degree of fuel stratification and spray/wall interaction, which is unavoidable in small-bore passenger vehicle engines (Kaiser *et al.*, 1999). The impingement of liquid fuel on the combustion chamber wall is generally undesirable in DISI engine because it increases HC emissions and affects the combustion phasing during acceleration transients. However, with a wall-guided stratified-charged combustion mode at late injection, the impingement of gasoline spray on the piston wall is intended in order to divert the rich mixture to spark plug for successful ignition and stable combustion.

Therefore there is a great need to characterize the DISI gasoline spray-wall interaction in detail, not only to understand the fundamental transport processes, but also to provide data to validate CFD predictions, which have become indispensable in the design of DISI engines.

Fuel economy improvement, potentially up to 30%, is the main driving force behind the recent research and development push toward direct injection spark-ignition (DISI) engines by automotive industry. DISI engines also have potential for significantly improved drivability (transient response, power performance), downsizing benefits,

**Corresponding author.* e-mail: ksim@wayne.edu

cold start emissions over port fuel injection (PFI) engines. Although complexity in combustion and emissions control, excessive light-load UBHC and high-load NO_x emissions are among their main drawbacks.

2. EXPERIMENTAL SETUP

The test setup includes a heated pressurized chamber designed for optical access, a heated aluminum disk, and a DISI injection system. The aluminum disk is used as a heat capacitance, heated up to 170°C by a thin etched-foil heater on the back. Purging air flows slowly from the top of the chamber, heated by a 40 kW heater upstream and drained at the bottom of the chamber. A narrow-cone (α=20°) and a wide-cone (α=60°) high-pressure swirl gasoline injectors were used in the experiment. For simplicity, injection pressure remains at 4.8 MPa (700 psi gauge) throughout the experiment, causing slower, but slightly larger droplet diameter for better visualization. The injection duration is kept short, at 0.5 ms for narrow-cone injector and 2.0 ms for wide-cone injector to minimize optical obscuration by dense-spray at impingement. Premium gasoline is used as the fuel. The wall is located 38 mm directly below the injector tip. A total of five thermocouples monitor the temperature conditions: two for air, two for fuel temperature and one for plate temperature. Different air and the plate temperatures are chosen for the test conditions: For the cold cases, the temperature of the air and the plate is about the same as the ambient temperature; i.e., T_a=T_w=23±2°C. For the hot cases, the air is kept at T_a=95±5°C and the plate is kept at T_w=160±10°C. Two different wall impingement angles, θ=90° and θ=58° (as denoted by horizontal and inclined cases) are used. For the preliminary results presented in this paper, the chamber pressure is kept constant at around 335 kPa (absolute) except in the shadowgraph and PIV experiments, which are carried out at atmospheric pressure. The experimental conditions and instrumentations are summarized in Table 1.

The optical diagnostic systems include the followings; a copper-vapor laser and a ultra-fast spark discharge system as the light sources; long-distance microscopic lens, shadowgraph optics; and a CCD camera and high-speed 35 mm drum camera as imager. The copper-vapor laser beam is expanded into a thin sheet using cylindrical lens and is used as an optical shutter, up to 25 kHz, for the drum camera in the Laserstrobe system (Oxford Laser). The combination of the long-distance microscope (Questar QM100) with the Laserstrobe system has been used to visualize diesel spray before (Lai *et al.*, 1998). The resolution (measurable separation of a space between two bars on a resolution target) is about 1–2 microns at 15–30 cm away. The experimental setup with this system is arranged as shown in Figure 1.

Table 1. Experimental set-up.

	Category	Micro-scopic	Macro-scopic	PIV
Ambient air	T_a (°C)	23±2 for ambient 95±5 for hot		23±2
	P_a (kPa)	335		101.3
Injection	Injector	α=20°, 60° P_i=4.8 MPa		
	Duration (ms)	0.5 for 20° 2.0 for 60°		1
Plate	T_p (°C)	23±2 for ambient 160±10 for hot		
	Position	38 mm below the injector tip Horizontal (90°) or inclined (32°)		

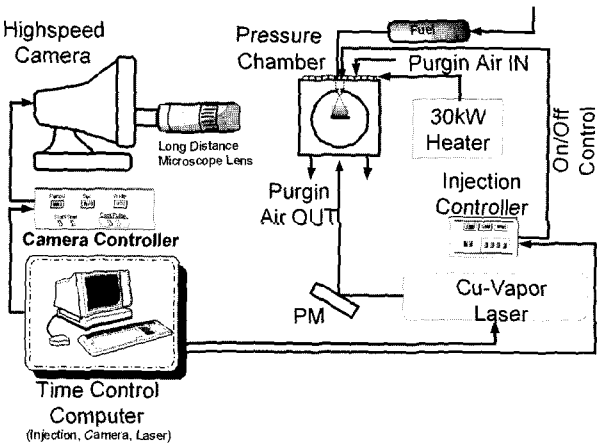

Figure 1. Macro/Microscopic visualization setup.

Particle Motion Analysis System (PMAS by Vtek) is used to obtain the shadowgraph and PIV visualization results and is shown in Figure 2. The ultra fast spark light

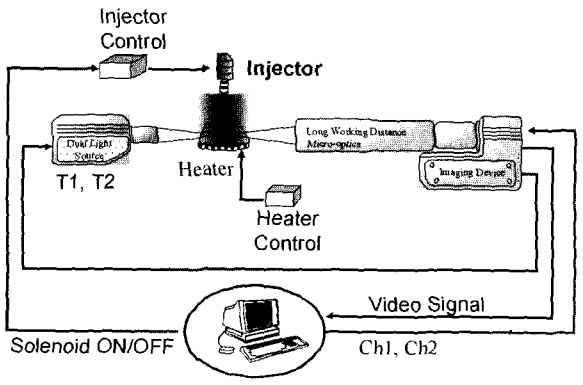

Figure 2. Shadowgraph and PIV experiment setup.

source generates a 50-ns spark with an energy output of about 1.5 Joules. It also has double-pulse (minimum separation of 1 μs) capability for use in particle image velocimetry (PIV) applications. This light source combines with a microscopic lens and a CCD camera, in an integrated system (Vtek PMAS) for spray imaging and dropsize/velocity analysis.

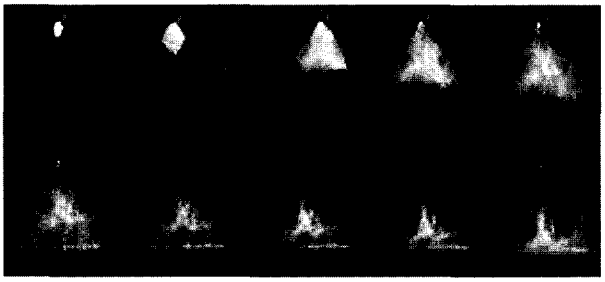

(a) θ=90°, cold case (Ta=Tw=23°C)

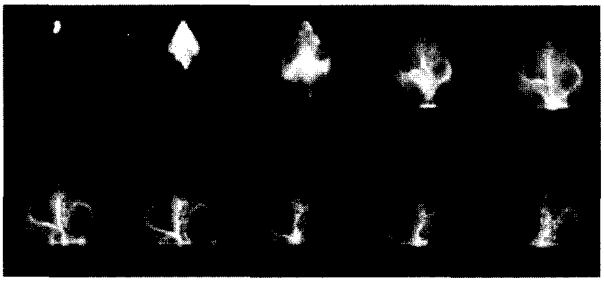

(b) θ=90°, heated case (Ta=95°C, Tw=160°C)

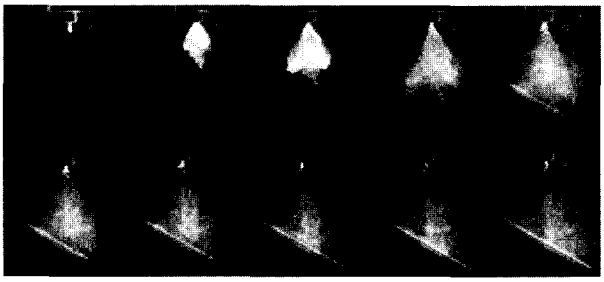

(c) θ=58°, cold case (Ta=Tw=23°C)

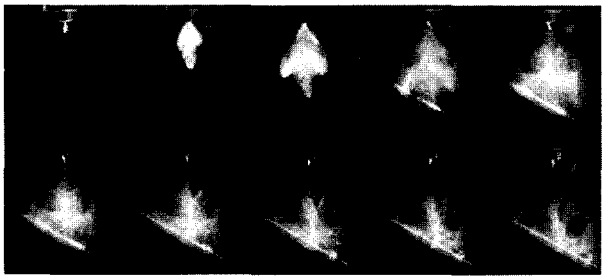

(d) θ=58°, heated case (Ta=95°C, Tw=160°C)

Figure 3. High-speed light-sheet visualization for wide-cone spray (α=60°) and impingement. The injection duration, Δt, is 0.5 ms. The first frame begins at t_1=0.41 ms after the start of injection driver pulse, time increment between each frame is 0.1 ms.

3. RESULT AND DISCUSSIONS

3.1. Macroscopic Visualization

Figures 3 and 4 show the macroscopic visualization for the wide- and narrow-cone injectors, respectively, at various temperature and impingement angle conditions. The injection duration, Δt, is 0.5 ms. The time separation between each frame is 0.1 ms. Each frame in Figures 3 and 4 has a 50.7 mm-by-63.3 mm field-of-view.

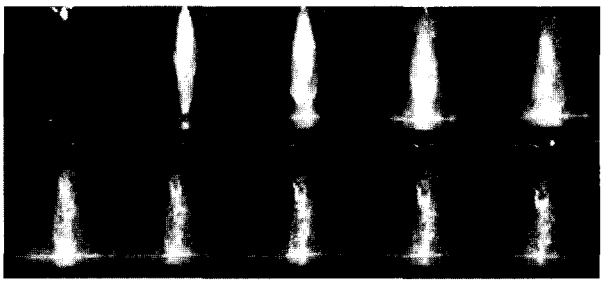

(a) θ=90°, cold case (Ta=Tw=23°C)

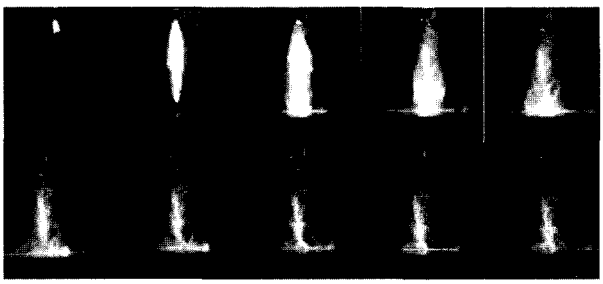

(b) θ=90°, heated case (Ta=95°C, Tw=160°C)

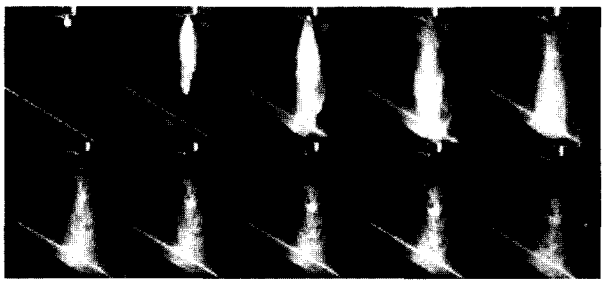

(c) θ=58°, cold case (Ta=Tw=23°C)

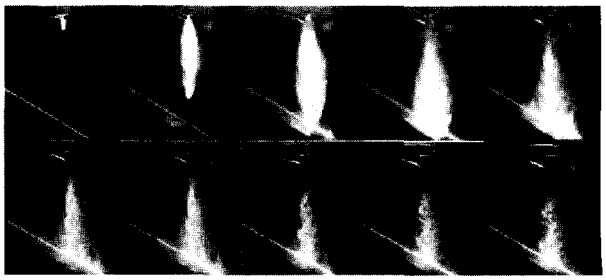

(d) θ=58°, heated case (Ta=95°C, Tw=160°C)

Figure 4. High-speed light-sheet visualization for narrow cone spray (α=20°) and impingement, under the same conditions as in Fig. 3.

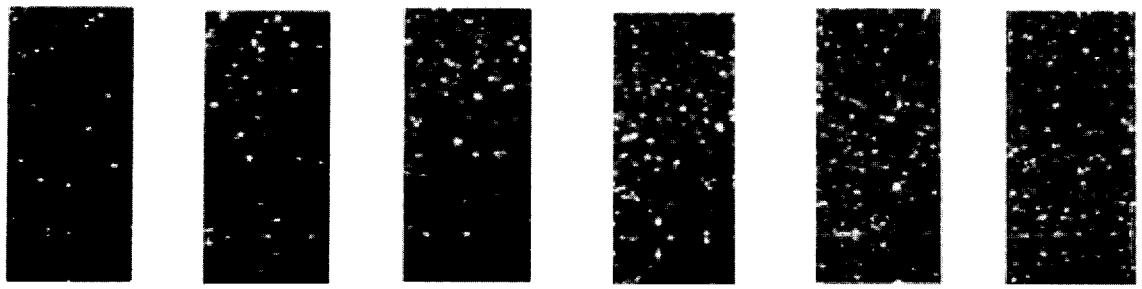

(a) α=60°,θ=90°,Δt=2ms,cold,r=20mm,t_1=1.64ms

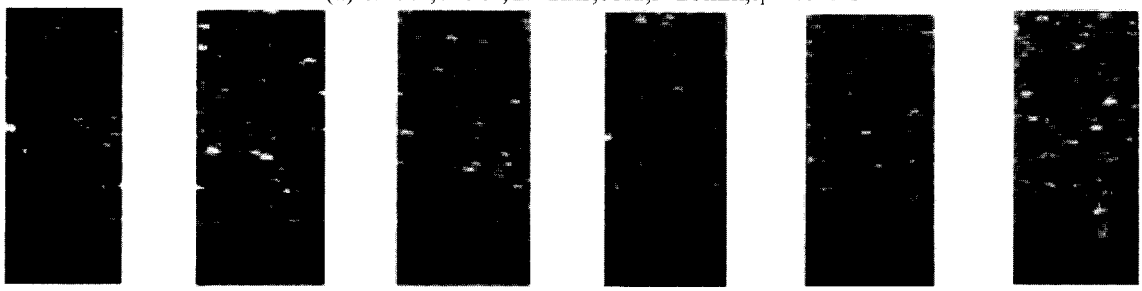

(b) α=60°,θ=90°,Δt=2ms,heated,r=20mm,t_1=2.6ms

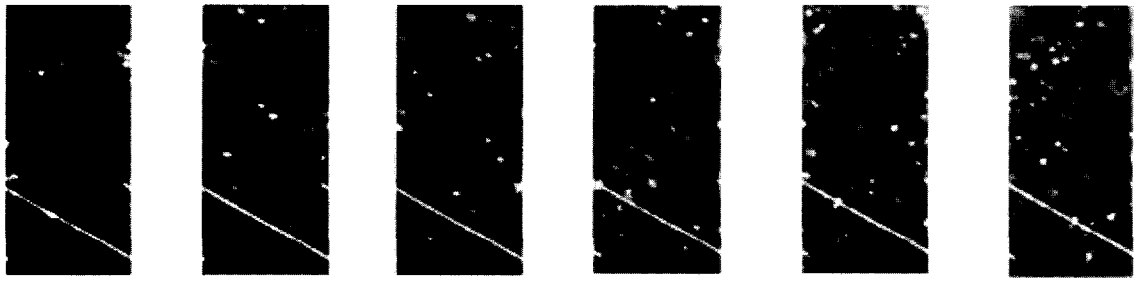

(c) α=60°,θ=58°,Δt=2ms,cold,r=20mm,t_1=2.28ms

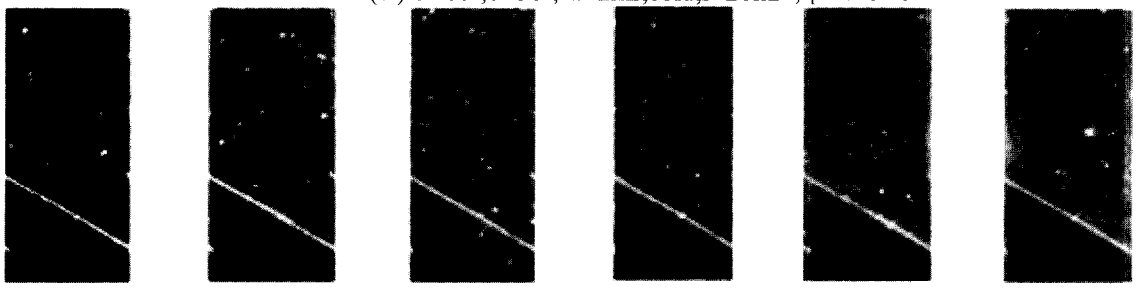

(d) α=60°,θ=58°,Δt=2ms,heated,r=20mm,t_1=1.96ms

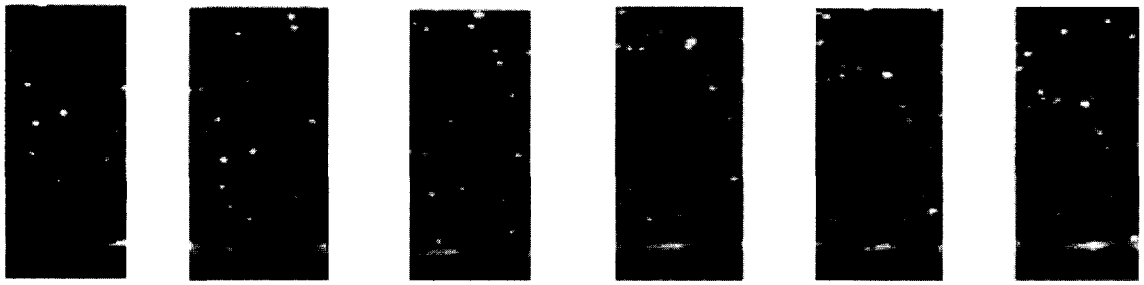

(e) α=20°,θ=90°,Δt=0.5ms,cold,r=6mm,t_1=2.89ms

Figure 5. Sample high-speed microscopic visualization of spray wall impingement; time increment is 0.04 ms; starting time varies, as indicated; each frame has 1mm-by-2mm field of view.

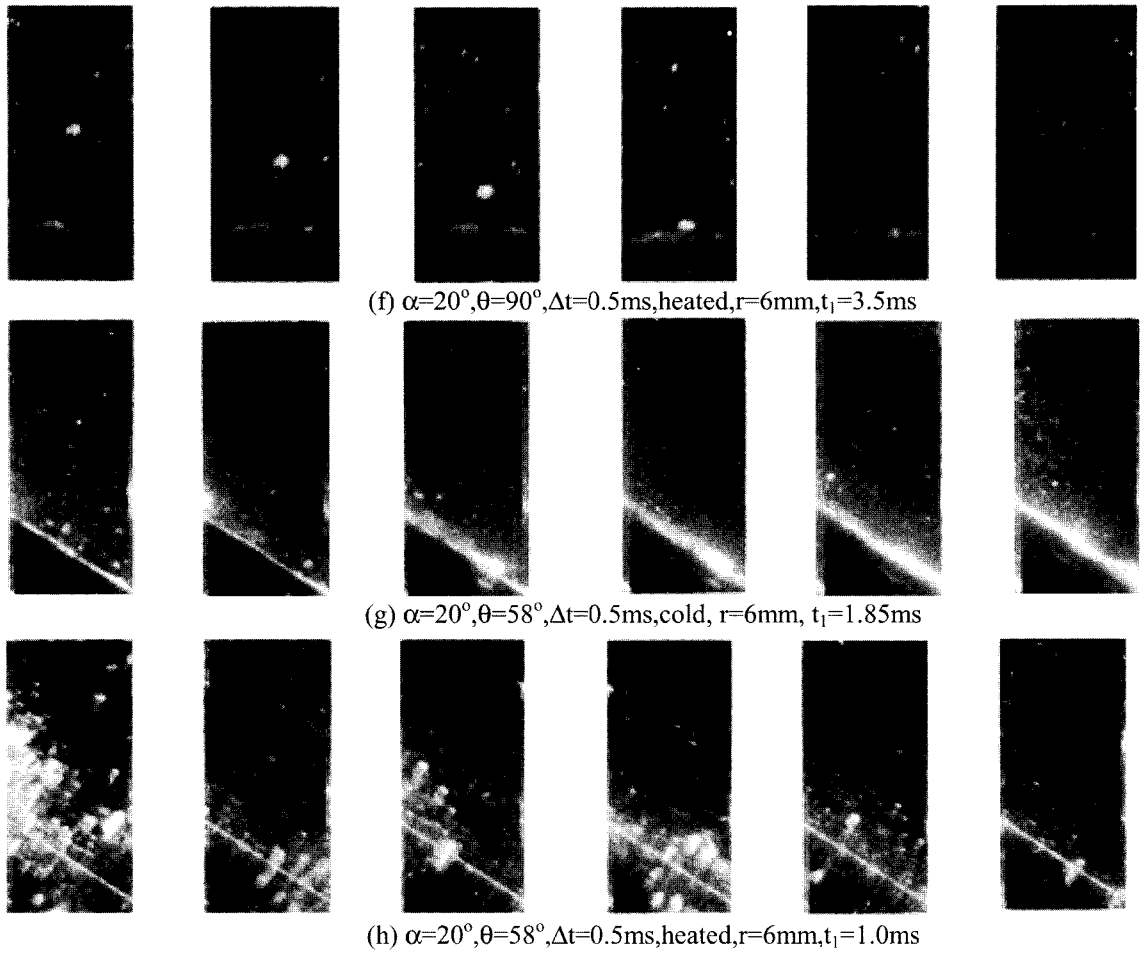

Figure 5. Continued.

Overall spray structure appears to be similar between the cold and hot cases, horizontal and inclined plate cases; however, a closer examination shows that the initial spray front (due to sac volume effect) is more obvious and penetrates slightly faster in the heated case, especially for the wide-cone spray. In addition, the upward spray vortex is distinctively more vigorous before and after wall impingement at elevated-temperature conditions. This is due to the vaporization of small-size droplets, making the sac spray and vortex structure more obvious. The increased air viscosity and decreased air density at elevated temperature may also contribute to these effects. Compared to the wide-cone injector, the impingement intensity is more forceful and focused for the narrow cone injector, as expected.

The vortex inside the spray is not clearly observed for the 20° injector due to the more concentrated spray density; however, the spray density is lower for the heated cases, showing more skeleton features because of vaporization. Fuel film is observed to coat the surface at both horizontal and inclined wall conditions. In the inclined wall cases, the spray plume has a tendency to slip along the wall especially at cold wall temperature. For both wide and narrow cone injectors, macroscopic visualization results show different vigorous spray/wall interactions, but do not directly show the details of droplets rebounding; therefore, microscopic visualization techniques are required to show the details of spray impingement, droplet splashing or break-up, and film formation.

Figure 5 shows some sample digitized film clip sections from the entire microscopic visualization. The laser is running at 25 kHz, therefore, each frame is 0.04 ms apart. The starting time of each film clip (t_1) varies as indicated in the figure. It is chosen at each condition to represent the best visual correlation between frames. The wall surface reflects the incoming droplets like a mirror when it is relatively dry. When the wall becomes wet or during active vaporization near the surface, it becomes too fuzzy to reflect. The inclined wall surface is easier to visualize since it blocks laser light passage, and reflects.

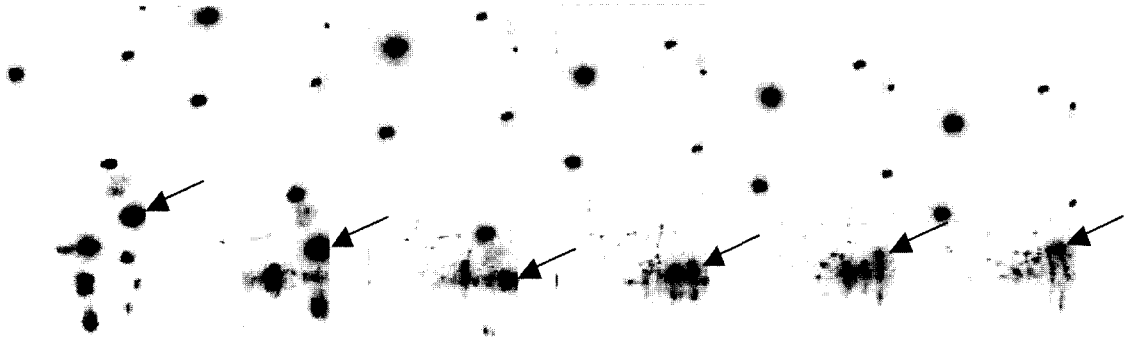

Figure 6. Hi-speed microscopic visualization showing rebounding; $\alpha=60°$, $\theta=90°$, $\Delta t=2$ ms, cold, $r=20$ mm, $t_1=0.65$ ms. time increment is 0.04 ms.

It is interesting to see the growth of film-build even on the heated surface. For the wide-angle spray, the film-build remains very thin because of a wider impingement area, accumulating relatively small amount of fuel in the visualization area. It also seems to disappear quickly after the droplets hit, due to vaporization. The film-build for the narrow cone is much more obvious, up to 100-micron thick from images in Figure 5(g). Figure 5(f) and (g) also show that the spray plume and liquid film have a tendency to slip along the wall, consistent with the macroscopic visualization results.

It is clear that 0.04 ms time separation is generally too long for particle trajectory velocimetry (PTV) analysis especially when the spray is fast, i.e., during the bulk spray impingement period. Only when the spray is slow, such as in Figures 5(e), 5(f), and 6, which are at the tail ends of the spray processes, or when a big droplet with a low speed is captured, the frame-to-frame correlation become better (Lai *et al.*, 1995). For these cases, the impingement velocity is slow, droplets either stick on the wall as shown in Figure 5(e), 5(f), or rebound as shown in Figure 6. Droplet impingement behavior can be analyzed by calculating pre- and post-impingement Weber numbers.

Figure 6 shows one type of rebounding behavior of a big fuel droplet, assumably due to the sac volume effect. Upon reaching the impingement surface, the droplet disintegrates into smaller droplets. A part of disintegrated liquid fuel droplet vaporizes. Remaining portion of disintegrated part rebounds with relatively slow upward speed with a ligament tail still attached to the impingement surface for a short time after impingement. This ligament tail is latter broken into smaller droplets keeping the shape of its trail from the impingement surface, and finally vaporizes leaving only the nuclei of the rebounded particle. However, in order to find good correlation of particles between two consecutive 1mm × 2mm images separated by 0.04 ms, the speed of droplets must be significantly less than 50 m/s.

Therefore, PIV analysis is carried out instead using the double-pulsed spark PMAS system, which has shorter time separation but is limited to only one doubly exposed image and lose the temporal continuity of the movies.

3.2. Shadowgraph and PIV Results

Figure 7 compares the spark shadowgraphs of the narrow cone spray (α=20°) impinging onto a cold plate (T_w= 23°C) on the left side, with those onto a heated plate

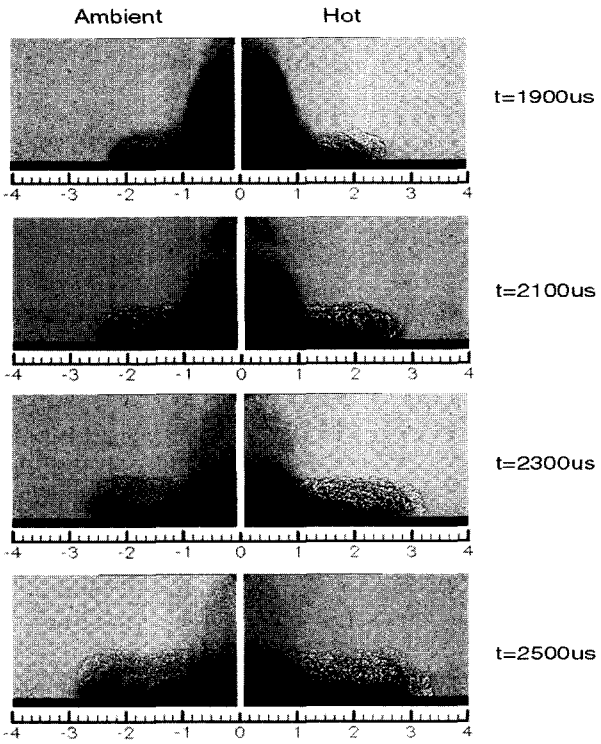

Figure 7. Shadowgraphs of the narrow-cone spray impinging onto a cold plate (left, T_w=23°C) and onto a heated plate (right, T_w=160°C). Injection duration Δt=1 ms, imaging time from top to bottom: 1.9, 2.1, 2.3, 2.5 ms.

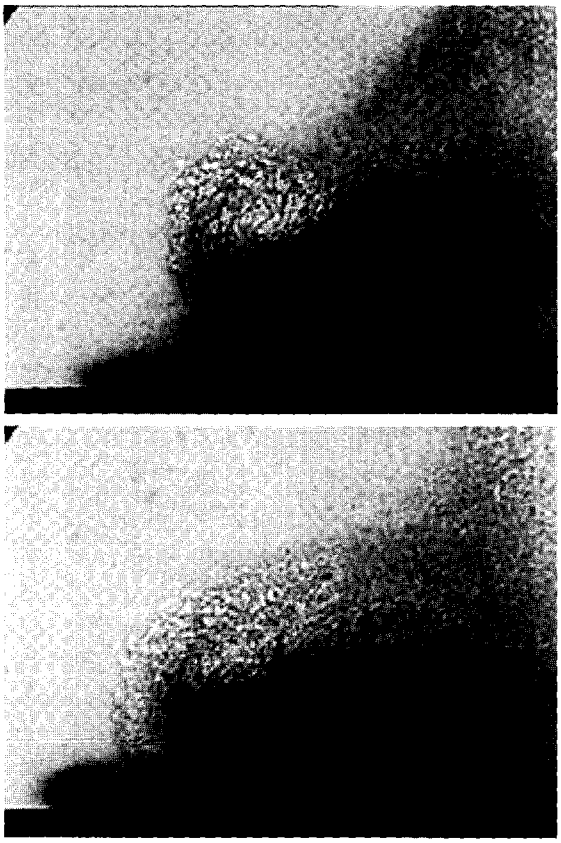

Figure 8. Shadowgraph of the wide-cone spray impingement propagation onto a cold plate. Injection duration Δt=1 ms and imaging time is 2.2 ms for the top figure, 2.5 ms for the bottom figure after injection. Images shown have a dimension of 1.2 (H)×1.5 (W) mm.

(T_w=160°C) on the right side taken at the same time step. These images were taken using Vtek system under ambient pressure condition, without the ambient air. The injection duration was 1ms, the imaging time are 1.9, 2.1, 2.3 and 2.5 ms from top to bottom. The liquid phase shows up as fine dark dots within the silhouettes, while the vapor phase is manifested as layered eddy structure. Even for the unheated case, vapor phase also appears in the impingement zones and in the wake of fuel spray, as the lighter and more volatile components in the gasoline fuel vaporize. The heated plate clearly shows more rapid vaporization and faster horizontal spread of the fuel plume after impingement, although the height of the vapor phase plume appears to be the same as in the unheated case.

Figure 8 shows the two-phase (Vapor and liquid) propagation after impingement using shadowgraphic technique for wide-cone injector. Vortex formed at the edge of the spray approximately 1.2 ms after injection, containing strong fuel vapor contents. Closer to the wall, a layer of

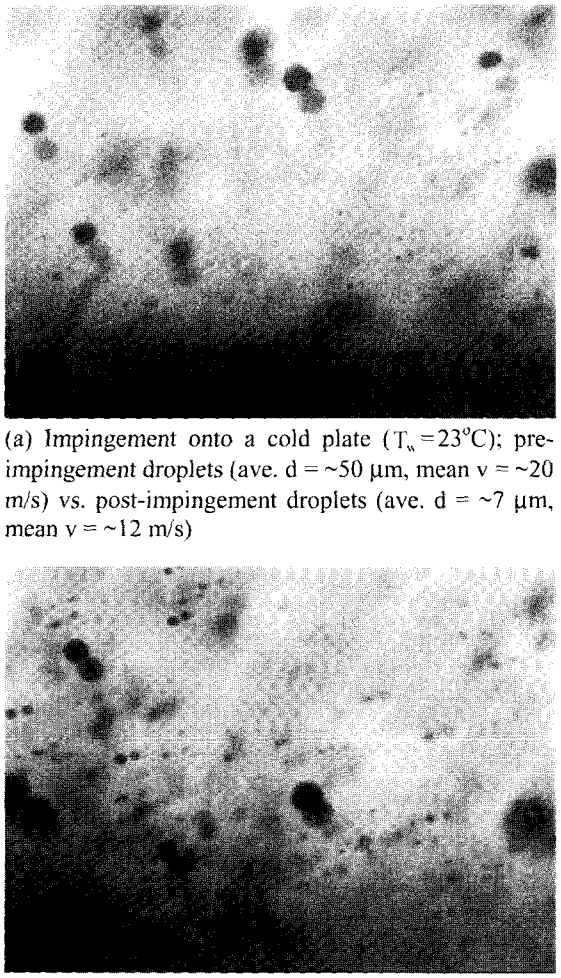

(a) Impingement onto a cold plate (T_w=23°C); pre-impingement droplets (ave. d = ~50 μm, mean v = ~20 m/s) vs. post-impingement droplets (ave. d = ~7 μm, mean v = ~12 m/s)

(b) Impingement onto a hot plate (T_w=160°C); pre-impingement droplets (ave. d = ~40 μm, mean v = ~25 m/s) vs. post-impingement droplets (ave. d = ~13 μm, mean v = ~14 m/s)

Figure 9. Microscopic PMAS visualization of the wide cone spray (α=60°); injection duration Δt=1 ms, imaging location 21 mm from the center.

wall-jet-like spray propagates and grows along the wall, within only 0.2 ms.

Figure 9 shows the PIV result using PMAS from the wide-cone angle injector. The doubly-exposed images depict many droplet pairs with the first exposed droplet images darker than the second ones. This enable us to determine the velocity vectors of the droplet if the image pair is sharp; i.e., located within the 1.5 mm-deep focal plane. PIV analysis for Figure 9 is performed and shown in the legend. PMAS tends to visualize only larger droplets. For example, the preliminary PDPA results show that the average droplet diameter for pre-impingement, moving toward the wall, is between 16 μm and 23 μm, while for post-impingement, moving away from the wall,

is between 12 μm and 20 μm. Especially in the presence of large droplets such as in pre-impingement, the average droplet diameters that PMAS analyzed are about twice of the diameter analyzed by PDPA.

Figure 9 clearly shows that several large pre-impingement droplets impinge with an angle approximately 60 degree from the horizontal plate, disintegrate into smaller droplets, and rebound with smaller angles in a field-of-view of 1.2×1.5 mm. Figure 9 also shows that droplet rebounding is more vigorous at elevated temperature. Additionally, the left lower corner of Figure 9(a) shows a trace of a ligament formation after impingement, which confirms the finding about ligament formation and break-up from the microscopic visualization in Figure 6. Some researchers previously concluded in their impingement model that a liquid film formed by droplet impingement breaks up by following bombardment of another droplets, causing a column type breakup, which is very similar to ligament formation and break-up visualization results presented in this paper (Senda *et al.*, 1999). From Figure 7, 8, and 9, the post-impingement droplets were observed to move horizontally than vertically compared with pre-impingement ones. This phenomenon is due to the entrained airflow which changes direction of the post-impingement droplets and moves them more tangent to the surface (Naber *et al.*, 1988), and the post-impingement droplets have relatively smaller diameters and they tend to follow the airflow. In addition, PMAS results show that post-impingement droplets are significantly smaller and slower than pre-impingement ones.

Figure 10 shows the doubly-exposed microscopic PMAS visualization taken at three different locations, as marked out on the shadowgraph. The test condition is the same as in Figure 6. All images shown in Figure 8 were taken at the same time: 0.93 ms after injection driver pulse, which is during the early impingement period. Area (a) shows a very active spray impingement process, with many large droplets presumably coming from either the sac volume effects or from droplets splashing from the liquid film-build. However, dense spray in this region makes further analysis difficult by blocking the optical path. Area (b) shows a much smaller droplet (ca. 20 microns SMD) with a fast horizontal velocity component (ca. 30-40 m/s) which is from the post-impingement droplets. Area (c) is at the very front of the fuel plume, showing even smaller droplets moving at slower speed (ca. 20-30 m/s).

The series of microscopic visualization Figure 10(a), (b), and (c) taken by PMAS system indicates that after droplets impinge the wall, they disintegrate into smaller droplets, then rebound with a more horizontal velocity component while vaporizing at the same time. Impinging droplets in this experiment have Weber numbers over 400. This result confirms the findings from other researches

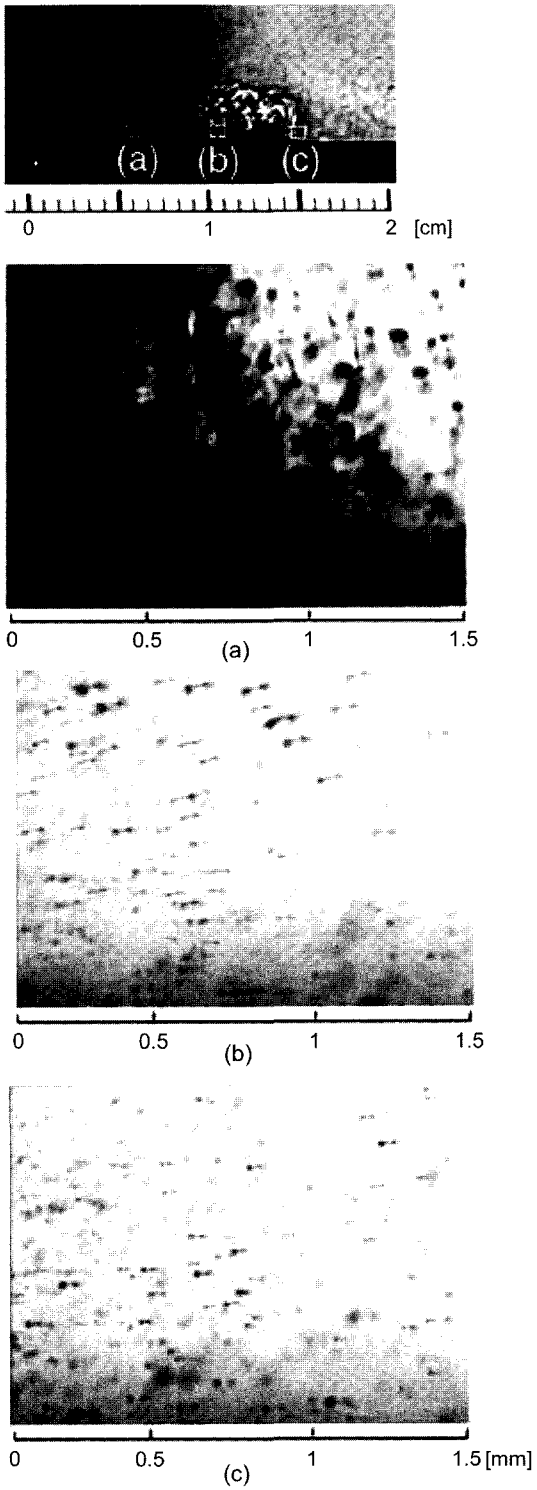

Figure 10. PIV results at 3 different locations.

that droplets having Weber number higher than 300 would follow splash type break-up process of the film formed on the surface (Senda *et al.*, 1999). Droplet

Weber number has significant meaning since it defines the relationship between droplet momentum and surface tension, thus predict the droplet break-up process. The larger drop size and Weber number calculated from this experiment could partially due to the slightly lower injection pressure compared with usual DISI injection pressure, which is approximately 4 to 10 Mpa (Zhao *et al.*, 1997). Tendency to visualize large droplets by the PMAS equipment could also cause larger Weber number calculation. Droplets from sac volume are another possibility of producing large droplet diameters in the short injection duration (0.5~1.0 ms) used in this experiment.

A single-droplet experiment by Wachters *et al.* (1966) confirms that a droplet with impinging Weber number over 80 disintegrates and spreads along the wall, which agrees well with the findings from this experiment.

Sample droplet Weber number analysis for the wide-cone injector impinging onto the horizontal plate is shown in Figure 11, based on the PMAS image taken at 21 mm from the center of the injection. Generally speaking, Weber numbers for the droplets impinging onto the hot plate are larger than those impinging onto the cold plate, possibly due to vaporization of the smaller droplets. Also, decreased air density due to the heated plate probably contributes to the faster droplet velocity, which in turn, results in higher Weber number. Pre-impingement droplets have larger Weber number than post-impingement droplets because the size and the speed for pre-impingement droplets are larger than those of post-impingement droplets. Preliminary droplet Weber number analysis based on PMAS microscopic analysis shows that most droplets impinge, disintegrate, and rebound upon the impingement, and this phenomenon is more distinct at elevated plate temperature.

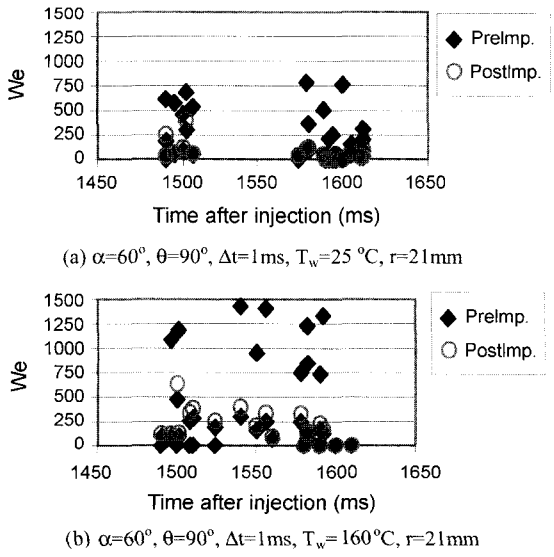

(a) α=60°, θ=90°, Δt=1ms, T_w=25 °C, r=21mm

(b) α=60°, θ=90°, Δt=1ms, T_w= 160 °C, r=21mm

Figure 11. Weber number analysis for wide-cone spray.

4. CONCLUSION

Various visualization techniques, including high-speed macroscopic and microscopic movies, spark-shadowgraphy, and doublespark particle image velocimetry are used to characterize the DISI gasoline spray/wall interactions. The results obtained using these techniques are valuable resources to study the complex spray impingement processes. The results are summarized as follows:

(1) Macroscopic Visualization

Overall spray structure including spread angle is very similar for the different temperature and impingement condition tested, but spray penetration speed for wide cone spray is slightly higher at elevated temperature condition. Upward spray vortex inside the spray is more obvious at elevated temperature condition due to the vaporization of small droplets and decreased air density. This effect is particularly more visible in wide-cone-angle injector.

Fuel film is observed to form on the impingement location for both horizontal and inclined wall conditions for narrow cone injector. Rapid plume and liquid film moving along the wall is distinctly observed in the inclined case at ambient temperature.

(2) Microscopic Visualization

Film build-up on the surface is clearly observed at both ambient and elevated temperature especially for narrow cone spray. However, time separation (0.04 ms) between the frames is too large for particle trajectory velocimetry (PTV) analysis. However, some large droplets impinging at slower velocity shows splashing and rebounding phenomena.

(3) Shadowgraph and PIV

Vapor phase appears at both ambient and elevated temperature conditions, particularly in the toroidal vortex and impingement plume. More rapid vaporization and faster horizontal spread after impingement are observed for elevated temperature conditions, while the height of the vapor phase in the impingement plume above the surface appears to be similar for both temperature conditions.

Droplet rebounding and film break-up are clearly observed. Post-impingement droplets are significantly smaller than pre-impingement droplets with a more velocity component horizontally regardless of the wall temperature and impingement angle condition.

Preliminary Weber number results based on PMAS analysis has a wide range, up to 1,500. The Weber

number is shown to be reduced after impingement. However, the Weber number for the heated case appears larger due to vaporization of small droplets.

ACKNOWLEDGEMENT–The financial support from the Ford Motor Company and equipment grant from the VTek Inc. are appreciated to carry out the experiments described above.

REFERENCES

Kaiser, E. W., Siegl, W. O., Brehob, D. D. and Haghgooie, M. (1999). Engine-out emissions from a direct-injection spark-ignition (DISI) Engine. *SAE Paper No.* 1999-01-1529.

Kim, H., Im, K.-S. and Lai, M.-C. (2004). Pressure modulation on micro-machined port fuel injector performance. *Int. J. Automotive Technology* **5, 1,** 9-16.

Lai, M.-C., Chue, T.-H. and Li, L. (1995). Comparisons of venturi nozzle spray measurements using PDPA, PIV and PTV. *ILASS AMERICAS '95.*

Lai, M.-C., Wang, T.-C. and Xie, X. (1998). Microscopic visualization of the diesel spray behavior. *ILASS AMERICAS '98.*

Naber, J. and Reitz, R. D. (1988). Modeling engine spray/wall Impingement. *SAE Paper No.* 880107.

Naber, J. D. and Farrel, P. V. (1993). Hydrodynamics of droplet impingement on a heated surface. *SAE Paper No.* 930919.

Nagaoka, M., Kawazoe, H. and Nomura, N. (1994). Modeling fuel spray impingement on a hot wall for gasoline engines. *SAE Paper No.* 940525.

Senda, J., Ohnishi, M., Takahashi, T., Fujimoto, H., Utsunomiya, A. and Wakatabe, M. (1999). Measurement and modeling on wall wetted fuel film profile and mixture preparation in intake manifold for SI Engine. *SAE Paper No.* 1999-01-0799.

Wachters, L. H. J. and Westerling, N. A. J. (1966). The heat transfer from a hot wall to impinging water drops in the spheroidal state. *Chemical Engineering Science,* **21**.

Yoo, J., Kim, S., Zhao, F.-Q., Lai, M.-C. and Lee, K.-S. (1998). Characterization of direct injection gasoline sprays in different ambient and wall impingement conditions. *SAE Paper No.* 982702.

Zhao, F.-Q., Lai, M.-C. and Harrington, D. L. (1997). A review of mixture preparation and combustion control strategies for spark-ignited direct-injection gasoline engines. *SAE Paper No.* 970627.